JOURNAL OF Materials CHEMISTRY

Dielectric, structural and ferroelectric properties of strontium borate glasses containing nanocrystalline bismuth vanadate

N. Syam Prasad and K. B. R. Varma*

Materials Research Centre, Indian Institute of Science, Bangalore-560 012, India. E-mail: kbrvarma@mrc.iisc.ernet.in

Received 19th December 2000, Accepted 10th May 2001
First published as an Advance Article on the web 29th May 2001

Glasses of the composition $(100-x)\,SrB_4O_7$ (SBO)$-x\,Bi_2VO_{5.5}$ (BiV) ($0 \leqslant x \leqslant 70$) were fabricated by the splat quenching technique. The evolution of nanocrystallization of bismuth vanadate in the system 50 SBO–50 BiV (in mol%) was accomplished *via* controlled heat-treatment (in the temperature range 470–820 K) of the as-quenched glasses. Differential thermal analyses were performed to assess the glass transition (T_g) and crystallization temperatures (T_{cr}). X-Ray powder diffraction studies (XRD) confirmed the as-quenched samples to be amorphous. High resolution transmission electron microscopic (HRTEM) studies corroborated the XRD studies and indicated the BiV crystallite size in 720 K heat-treated composites to be around 15 nm. The dielectric constant (ε_r) and the dielectric loss (D) were measured in the frequency range 100 Hz–10 MHz at different temperatures (300–900 K). The dielectric constant of the glass nanocomposite (GNC) under study was predicted using various dielectric 2mixture formulae at 300 K and found to be in close agreement with that obtained using the Maxwell and logarithmic mixture rules. The samples that were heat-treated at two different temperatures, 720 and 820 K, exhibited broad dielectric anomalies in the vicinity of ferroelectric-to-paraelectric transition temperature of the parent BiV ceramics. Diffuseness of the observed transitions were estimated using Curie–Weiss formalism. The *P vs. E* hysteresis loops exhibited by GNC samples at high temperatures (670–760 K) demonstrate their ferroelectric nature.

Introduction

The physical properties and nature of phase transitions in polycrystalline electroceramics are known to be influenced by the size and morphology of the crystallites. Compressive or tensile stresses that arise as a result of microstructural changes would decrease or increase the ferroelectric-to-paraelectric transition temperature (T_c). In addition to simply shifting the transition temperature, stress fields can also influence the order of the phase transition through higher order elastic coupling coefficients. These trends are modeled using Devonshire phenomenological theory.[1] Grain size may also have strong influence on the broadening of the dielectric anomaly. Recently we have demonstrated the incidence of the diffuse ferroelectric-to-paraelectric phase transition in fine grained $Bi_2VO_{5.5}$ (BiV) ceramics, fabricated from the fine powders obtained *via* mechanical milling.[2] BiV is an interesting $n=1$ member of Aurivillius family ($A_{n-1}B_nO_{3n+1}$) of Bi-based layered structured oxides consisting of $[Bi_2O_2]^{2+}$ layers interleaved with pervoskite like sheets of $[VO_{3.5}\square_{0.5}]^{2-}$. It exhibits two polymorphs $\alpha \rightarrow \beta$ (725 K) and $\beta \rightarrow \gamma$ (840 K).[3]

The interesting feature of this compound is its polar property[4,5] and high ionic conductivity, which generally are incompatible in most ferroelectrics. The high ionic conductivity that is associated with γ-phase is attributed to the presence of random oxide ion vacancies in the pervoskite-like layers. The oxygen vacancies were disordered in the α- and β-phases of BiV and gave rise to a non-negligible ionic conductivity of the order of 10^{-6} to $10^{-3}\,\Omega^{-1}\,cm^{-1}$.[6] This is the major constraint in exploiting this material for polar device applications. One of the ways to reduce the ionic conductivity would be to dope the material with a suitable acceptor/donor impurity or alternatively one could achieve a decrease in ac conductivity or the dielectric loss (D) by modifying the microstructural features such as grain size, grain-to-grain contact and the grain boundary layers of these ceramics. Although there exist many ways to achieve this goal, the glass–ceramic composite route has been most effective, since amorphous solids offer a high degree of freedom in the topological and chemical arrangements of their constituent atoms. Further it is possible to tailor a material with a specific physical property by engineering the microstructure of a glass nanocomposite *via* a controlled heat treatment process. In the recent past several glass nanocomposites (GNC) have been fabricated in an aim to produce bulk materials consisting of nano/micrometer sized crystallites embedded in host glass matrices for multifarious applications. SrB_4O_7 (SBO) glasses by virtue of their thermal stability and wide optical transmission window associated with promising second harmonic intensity would form ideal glass host matrices for dispersing ferroelectric crystallites.[7,8] The basic interest in this work has been to study the structural, dielectric and polar properties of nanocrystals of BiV embedded in SBO glass matrices to be considered for possible device applications in lieu of single crystals.

In the present paper we report the results pertaining to the structural, thermal dielectric and ferroelectric characteristics of nanocrystalline BiV dispersed in SBO glass matrices of the representative composition 50 SBO–50 BiV, (in mol%), though we have investigated into the physical properties of other compositions, *i.e.* x ranging from 0 to 70 in the system $(100-x)\,SrB_4O_7$–$x\,Bi_2VO_{5.5}$.

Experimental

Glasses in the nominal composition $(100-x)\,SrB_4O_7$–$x\,Bi_2VO_{5.5}$ ($0 \leqslant x \leqslant 70$) were prepared by melting mixtures of prereacted strontium borate and bismuth vanadate in a platinum crucible at 1370 K for two hours. The pre-reacted samples (SBO and BiV) employed in the present studies were obtained *via* the conventional solid state reaction route involving strontium carbonate ($SrCO_3$), boric acid (H_3BO_3),

 DOI: 10.1039/b010120f

bismuth oxide (Bi_2O_3) and vanadium pentoxide (V_2O_5).[8,9] The melts were well shaken to ensure homogeneity and poured on a preheated (370 K) (to prevent the glass samples from cracking) stainless steel block and pressed by another to obtain flat plates (dimensions 1–2 mm thick, 1×1 cm^2 area). Subsequently all the samples under study were heat-treated at 425 K for 6 h, well before the glass transition temperature (T_g) to anneal out thermal strain that is likely to be associated with these samples. The as-quenched glassy samples and those heat-treated at various temperatures (470–1020 K) were examined by X-ray powder diffraction (XRD, SCINTAG) using Cu K_α radiation. The BiV phase formation in the heat-treated sample was confirmed by comparing its XRD data with that reported in the literature for BiV ceramic samples prepared by the conventional solid state synthesis route. A JEOL JEM 200CX electron microscope was employed for electron diffraction and high resolution transmission electron microscopy (HRTEM) of the as-quenched and heat-treated samples. The Archemedes method was used to determine the density (ρ), (thereby volume fraction) for both the as-quenched and heat-treated samples by using xylene as the immersion medium.

Differential thermal analyses (DTA) were carried out from 300 to 1020 K on the as-quenched and heat-treated samples by using a simultaneous thermal analyser (STA, 1500 Polymer Labs). The glassy nature of the as-quenched samples was confirmed by observing the glass transition (T_g) and crystallization temperatures (T_{cr}) in DTA traces. For this purpose a uniform heating rate of 15 K min^{-1} was employed for all the samples ($\approx$20 mg) under study. The capitance (C_p) and the dielectric loss (D) measurements were performed using a HP4194A Impedance/Gain phase analyzer in the frequency range 100 Hz–10 MHz. Polished surfaces of the plates (length = 10 mm, breadth = 9 mm, thickness = 1 mm) of the as-quenched and heat-treated glass–ceramic composites (50 SBO–50 BiV) were gold sputtered (to serve as electrodes, silver epoxy used to bond the leads) to make the capacitance measurements. To calculate the dielectric constant (ε_r) and dielectric loss dependency on temperature, capacitance and the dielectric loss (D), measurements were carried out in the temperature range 300–900 K using an indigenously built high temperature cell, interfaced with a personal computer. The dielectric constants were evaluated based on the capacitance, electroded area and sample thickness measurements. Ferroelectric hysteresis loops were recorded by using a modified Sawyer–Tower circuit[10] at a switching frequency of 50 Hz. For this purpose, the GNC samples were prepoled at 500 K by applying an electric field of 3.1 kV cm^{-1}.

Results and discussion

X-Ray powder diffraction and phase identification in the glass–ceramic composites

The XRD pattern for the as-quenched sample shown in Fig. 1(a) for the composition corresponding to 50 SBO–50 BiV confirms its amorphous state. However, the broad peak that is noticeable in this figure around the Bragg angle 2θ ($\approx 28^\circ$) corresponds to the most intense XRD peak of the parent polycrystalline BiV, confirming the presence of fine crystallites of BiV in the SBO glass matrix; indeed its full width at half maximum was found to decrease with increase in BiV content (not shown in this figure). In order to increase the amount of crystallization of BiV phase in the SBO glass matrix, the as-quenched glassy samples were subjected to heat treatment at various temperatures and durations to ascertain the crystallization and growth temperature of BiV. The X-ray powder diffraction obtained for the 720 K/8 h heat-treated 50 SBO–50 BiV glass–ceramic composite is shown in Fig. 1(b). The Bragg peaks that are encountered in this pattern could be indexed to an orthorhombic BiV phase associated with the

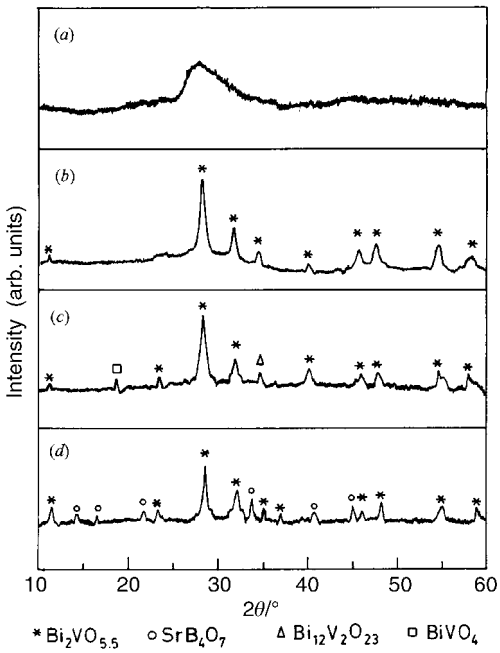

Fig. 1 XRD patterns for (a) as-quenched, (b) 720 K, (c) 820 K and (d) 1020 K heat-treated 50 SBO–50 BiV glass nanocomposites.

lattice parameters $a = 5.626$ Å, $b = 5.478$ Å and $c = 15.277$ Å, which are in good agreement with the values reported in the literature[4] for the parent polycrystalline BiV phase. At this stage, as evidenced from this figure no X-ray peaks that could be assigned to either crystalline SBO or any other impurity phase were present. However, the XRD pattern [Fig. 1(c)] that was obtained for the 820 K/8 h heat-treated sample revealed the presence of small amounts of impurity phases corresponding to $Bi_{12}V_2O_{23}$ and $BiVO_4$ apart from the major $Bi_2VO_{5.5}$ phase. In order to ascertain the temperature dependence of the stability of these minor impurity phases that are present along with the major BiV phase in the SBO glass matrix, the as-quenched glasses were heat-treated at 1020 K/8 h. The XRD pattern that was obtained at room temperature for this sample is shown in Fig. 1(d). It is interesting to note the absence of the impurity phases unlike in the previous case (820 K heat-treated). However, some additional Bragg peaks apart from that of the BiV phase are noted, which are attributed to the crystalline SBO phase indicating the onset of crystallization of the host SBO glass matrix at this level of heating. Thus, the systematic XRD studies confirm the crystallization of the BiV phase alone or of BiV with minor impurity phases, depending on the temperature range of heating of the as-quenched samples.

In order to pin down the exact heat-treatment temperatures that are required to obtain the crystallization of BiV in the SBO glass matrix, systematic DTA studies have been carried out on the as-quenched 50 SBO–50 BiV glasses. The DTA trace in the temperature range 300–1020 K that was obtained for the as-quenched sample is shown in Fig. 2(a). It exhibits four exotherms (marked as T_{cr1}, T_{cr2}, T_{cr3} and T_{cr4}) in the temperature range 690–980 K. Of these, the first and the fourth exotherms are strong. A sample that was heat-treated at a temperature 30 K above the first exotherm in Fig. 2(a) did not show an exotherm at 690 K on subsequent DTA analysis [Fig. 2(b)]. Similarly the glass that was heat-treated at 820 K, which is 30 K above the second exotherm did not exhibit this second exotherm on subsequent DTA analysis [Fig. 2(c)]. However, a clear endotherm corresponding to the glass transition temperature (T_g) of the sample is noted around 730 K. In order to understand the nature of the phase that is crystallized around the first, second, third and fourth

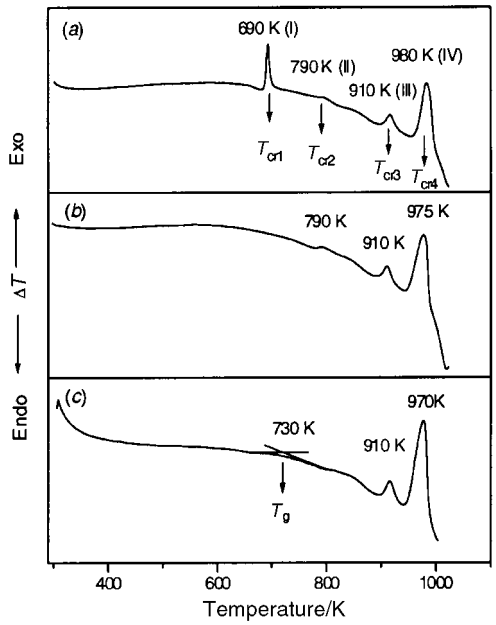

Fig. 2 DTA traces obtained for (*a*) as-quenched, (*b*) 720 K and (*c*) 820 K heat-treated 50 SBO–50 BiV glass nanocomposites.

exothermic temperatures, the glasses that were heat-treated around these temperatures were subjected to XRD studies. The results obtained on these samples are in accord with the XRD patterns of Fig. 1. Therefore, the first exotherm that is associated with the DTA trace shown in Fig. 2(*a*) is attributed to the crystallization of the BiV phase. The subsequent exothermic peak (II) is found to be associated with the crystallization of $Bi_{12}V_2O_{23}$ and $BiVO_4$ impurity phases [Fig. 1(*c*)]. The third exotherm that is encountered at 910 K is suspected to be associated with the reformation of BiV as a result of the reaction between $Bi_{12}V_2O_{23}$ and $BiVO_4$. Further the exotherm (IV) at 980 K, observed in Fig. 2(*a*) is attributed to the crystallization of the SBO host glass matrix phase based on XRD studies [Fig. 1(*d*)]. The interesting feature of these studies is the absence of impurity phases such as $Bi_{12}V_2O_{23}$ and $BiVO_4$ in the 1020 K (*i.e.* well beyond the IV exotherm) heat-treated sample. Based on DTA, combined with XRD studies, we propose that these impurity phases react chemically within the glass matrix of SBO and give rise to the required BiV phase according to eqn. (1);

$$10Bi_2VO_{5.5} \xrightarrow{820K} Bi_{12}V_2O_{23} + 8BiVO_4 \xrightarrow{910K} 10Bi_2VO_{5.5} \quad (1)$$

Transmission electron microscopy

The high resolution transmission electron micrograph of the as-quenched sample of composition 50 SBO–50 BiV is depicted in Fig. 3(*a*). The selective area electron diffraction (SAED) pattern, shown in the inset, demonstrates the overall amorphous nature of the as-quenched sample. The sharp haloes observed here arise from the presence of small crystallites (in the range 1–2 nm) of BiV in the host SBO glass matrix. The broad Bragg peak (in the XRD pattern), which was obtained for the as-quenched sample [Fig. 1(*a*)] corroborates this observation. The electron micrograph [Fig. 3(*b*)] along with the SAED pattern recorded for the sample heat-treated at 720 K for 8 h, indicates the presence of uniformly distributed spherical crystallites of nearly 15 nm size. The *d*-spacings, calculated from the SAED pattern [inset of Fig. 3(*b*)] for the 720 K heat-treated 50 SBO–50 BiV sample are in close agreement with that of a parent BiV polycrystalline sample. A high resolution lattice image of this sample is shown in the inset of

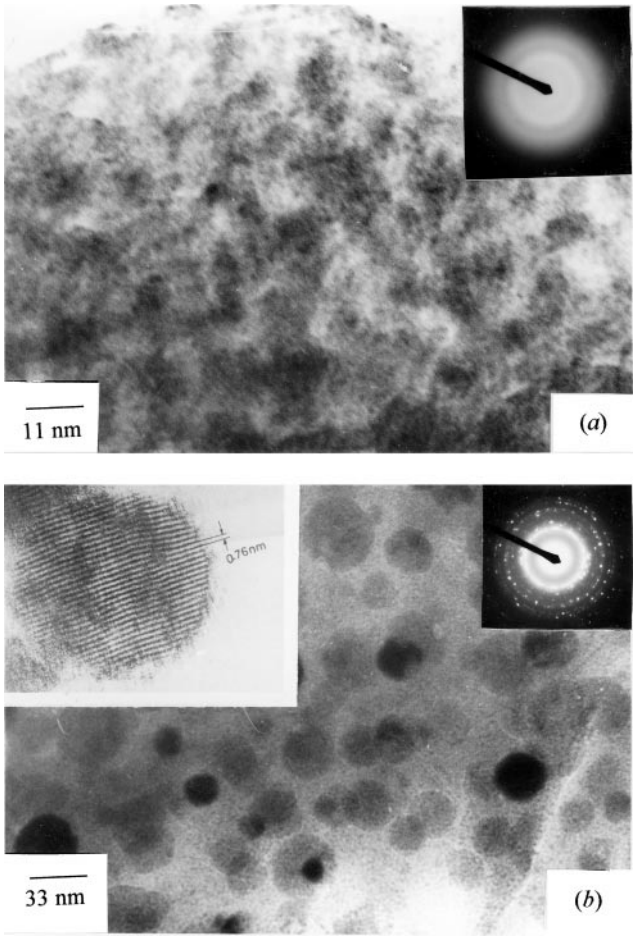

Fig. 3 TEM micrographs for (*a*) as-quenched and (*b*) 720 K heat-treated 50 SBO–50 BiV glass nanocomposites. Insets in (*a*) and (*b*) show the corresponding SAED patterns. A high resolution lattice image is shown in the inset of (*b*).

Fig. 3(*b*). The fringe spacing, observed in the crystallite, is 0.76 nm, which corresponds to one-half of the *c*-parameter of BiV.

Dielectric studies

The effect of heat treatment temperature in the range 470–820 K, on the density and the dielectric constant measured at 300 K are shown in Table 1. The density as well as the dielectric constant increase with increasing heat treatment temperature. The higher room-temperature value of dielectric constants of the heat-treated samples is attributed to the existence of strong dipolar interactions involved in the glass as the BiV crystallite size was found to increase with increase in heat treatment temperature.

Application of dielectric mixture formulae. The dielectric constant of a composite can be predicted by using different dielectric mixture formulae. Depending on the difference in the

Table 1 Density and dielectric constant (ε_r) for 50 SBO–50 BiV samples heat-treated at different temperatures

Heat-treatment temperature/K	Density/g cm^{-3}	Dielectric constant (ε_r) at 300 K (100 kHz)
470	5.001	18.4
570	5.014	18.8
670	5.061	19.3
720	5.166	20.1
820	5.274	36

dielectric constant of the constituents of the composite, dielectric loss, crystallite shape and their connectivity, one may use the Clausius–Mossotti, Maxwell, logarithmic, series and parallel mixture rule formalisms to estimate the value of ε_r of a composite. We applied these formulae for the present system 50 SBO–50 BiV (heat-treated at 720 K), containing BiV nanocrystallites with dielectric constant ε_1 (=90 at 100 kHz) and volume fraction δ_1 (=0.33), in the SBO glass matrix, which has a dielectric constant ε_2 (=10 at 100 kHz) and volume fraction δ_2 (=0.67).

In the Clausius–Mossotti treatment of a mixture of dielectrics composed of spherical crystallites dispersed in a continuous loss-less dielectric medium,[11] it is assumed that each inclusion is polarized independently, in a manner as if other inclusions were absent. The effective dielectric constant (ε_{eff}) of the composite is calculated using eqn. (2):

$$\varepsilon_{eff} = \varepsilon_2 \left[1 + 3\delta_1 \left(\frac{\varepsilon_1 - \varepsilon_2}{\varepsilon_1 + 2\varepsilon_2} \right) \right] \quad (2)$$

ε_{eff} obtained using this relation is 17.2 ± 0.5 (at 100 kHz, 300 K) and the experimentally measured value is 20.1 ± 0.5 (at 100 kHz, 300 K). Since, the volume fraction of BiV in SBO glass is reasonably high, the predicted value of ε_r is at variance with that of the experimental value.

The dielectric property of a diphasic dielectric mixture comprising of spherical crystallites with high dielectric constant dispersed in a matrix of low dielectric constant should be well described by Maxwell's model.[12] According to this model the effective dielectric constant of the composite is given by eqn. (3).

$$\varepsilon_{eff} = \frac{\delta_2 \varepsilon_2 \left(\frac{2}{3} + \frac{\varepsilon_1}{3\varepsilon_2} \right) + \delta_1 \varepsilon_1}{\delta_2 \left(\frac{2}{3} + \frac{\varepsilon_1}{3\varepsilon_2} \right) + \delta_1} \quad (3)$$

The calculated value using this model is 19.5 ± 0.5, which is close to the experimental value (20.1 ± 0.5).

According to the most commonly used dielectric mixture rule, eqn. (4),[13,14]

$$log\ \varepsilon_{eff} = \delta_1 \log \varepsilon_1 + \delta_2 \log \varepsilon_2 \quad (4)$$

which is also referred to as the logarithmic mixture rule and is the intermediate form of the series and parallel mixture formalism. ε_{eff} is 20.6 ± 0.5, which is remarkably close to the experimentally determined value 20.1 ± 0.5, for the present system. These results suggest that BiV crystallites are randomly distributed in the SBO glass matrix. A summary of the above results along with those obtained using series and parallel mixing rules are given in Table 2.

The frequency response of the dielectric constant (ε_r) along with that of the dielectric loss for the as-quenched glass nanocomposite of 50 SBO–50 BiV is shown in Fig. 4. The dielectric constant as well as the loss decrease rapidly in the low frequency region up to about 10 kHz and subsequently the dispersion with frequency is insignificant. It is very interesting to observe that for the as-quenched glass, the dielectric loss is less (0.013 ± 0.005) than that of BiV polycrystalline ceramic (0.8 ± 0.005) at 100 kHz. The Cole–Cole plots, that are

Table 2 Dielectric constants obtained using mixture rule formalism

Dielectric mixture rule formalism	Estimated dielectric constant at 300 K (100 kHz)
Clausius–Mossotti	17.2
Maxwell	19.5
Logarithmic	20.6
Series	36.4
Parallel	14.2
Experimental	20.1

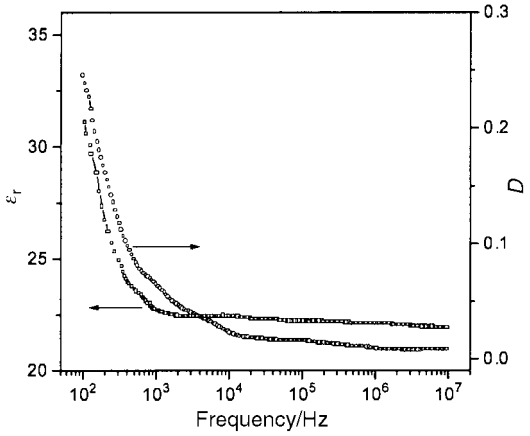

Fig. 4 Frequency response of dielectric constant (ε_r) and dielectric loss (D) for the 50 SBO–50 BiV glass nanocomposite heat-treated at 720 K.

generated between the real and imaginary parts of the dielectric constants confirm the nature of the direct relaxation that is associated with the present system to be non-Debye type. The full details of these studies will form a separate paper.

Temperature variation of dielectric constant and loss. The dielectric constant measurements that were made at three different frequencies on face electroded 720 K and 820 K heat-treated glass nanocomposites (SBO glass containing 15–40 nm crystallites of BiV as estimated using TEM studies) as a function of temperature are shown in Fig. 5(*a*) and (*b*). The corresponding temperature dependence of the dielectric loss (D) at three different frequencies (100 Hz, 1 kHz and 10 kHz)

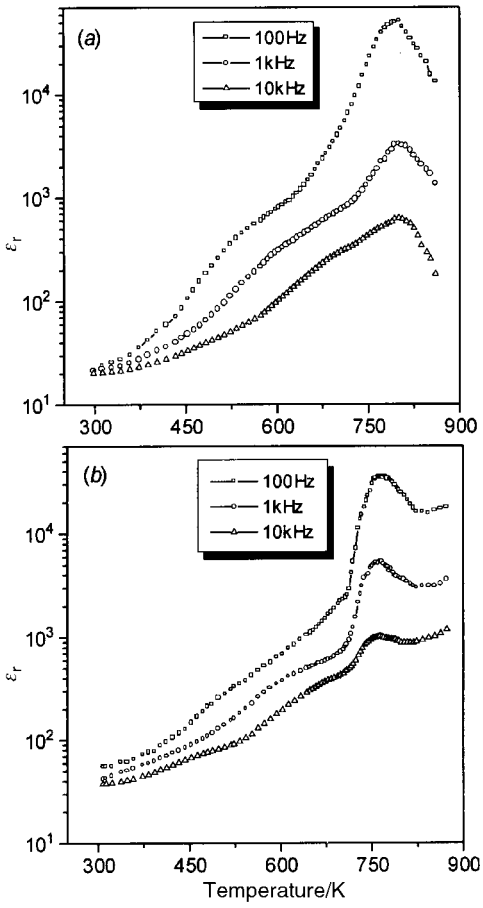

Fig. 5 Temperature dependence of ε_r at various frequencies for (*a*) 720 K heat-treated and (*b*) 820 K heat-treated 50 SBO–50 BiV glass nanocomposites.

for the samples heat-treated at 720 and 820 K are depicted in Fig. 6(*a*) and (*b*), respectively. The dielectric loss increases with increasing temperature and exhibits a peak at 680 K (100 Hz) for the 720 K heat-treated sample and shifts towards higher temperatures with increasing frequency (100 Hz–10 kHz) while for the 820 K heat-treated sample the dielectric loss exhibits two peaks in the range 740–830 K depending on the frequency of measurement. The first loss peak around 740 K for the 820 K heat-treated sample is close to that of its dielectric constant peak. Studies are in progress to understand the relaxation mechanism/s that is/are associated with these loss anomalies.

The dielectric constant in both cases increases monotonically with increase in temperature up to 700 K. Subsequently it increases rapidly at all the frequencies under study and reaches a maximum at 800 and 760 K for the 720 and 820 K heat-treated samples, respectively. These transition temperatures (though higher), occur around the ferroelectric-to-paraelectric transition temperature of polycrystalline BiV ceramic.[3] The higher T_c values in the present instances is attributed to the effects of the elastic and electrostrictive forces exerted by the surrounding glass matrix on the crystallites participating in the phase transition.

It is to be pointed out here that the transition temperature of the parent BiV ceramic was reported to be microstructure dependendent[15–19] and found to decrease with increase in crystallite size (in the μm range). The incidence of dielectric anomalies at 800 and 760 K for 15 nm (720 K heat-treated) and 40 nm (820 K heat-treated) BiV containing SBO glass matrices

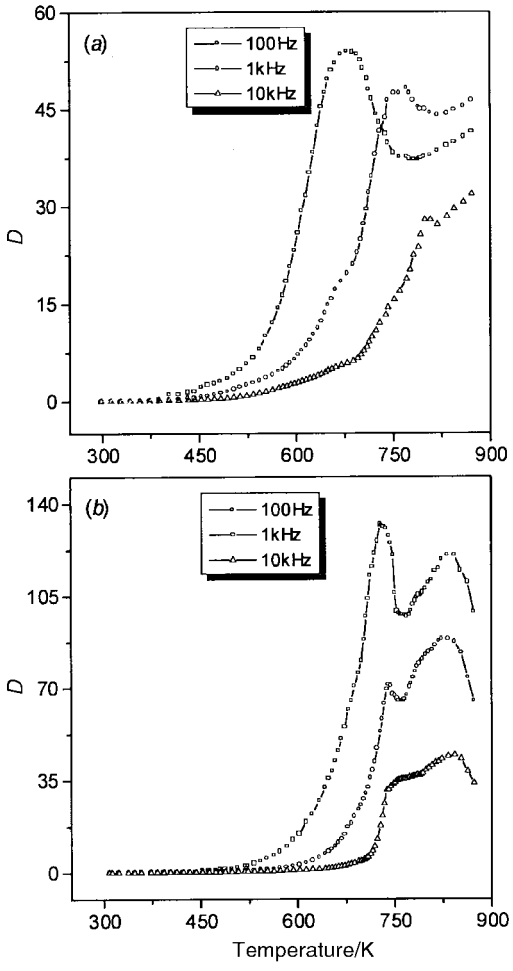

Fig. 6 Temperature dependence of D recorded at various frequencies for (*a*) 720 K heat-treated and (*b*) 820 K heat-treated 50 SBO–50 BiV glass nanocomposites.

suggest a decrease in transition temperature (T_c) with increase in crystallite size even in the nanometer range. However the principal difference lies in the nature of the transition which is diffuse and centered around 800 and 760 K for the 720 and 820 K heat-treated samples, respectively. In other words the transition exhibited by the present glass nanocomposites has a striking similarity with that of diffused type ferroelectrics.[20] The spread in the transition is significant enough for it to be considered of diffused type. The dielectric constant for the as-quenched sample (not shown in figure) also increases with an increase in temperature and reaches a maximum around 830 K. This anomaly in dielectric constant around 830 K can not be attributed to the crystallization temperature of the host glass matrix as it crystallizes at much higher temperatures (980 K).

The diffuse nature of the transition is ascribed to the existence of a nanosize distribution of BiV crystallites. The shifts in the transition temperature towards lower temperatures (tending towards the Curie temperature of parent polycrystalline BiV ceramic containing micrometer sized crystallites) with increase in crystallite size (15–40 nm range) is attributed to the decrease in tensile stresses in the composite. The broadness in the peak could be attributed not only to the crystallite size distribution (a similar trend has been observed in the dielectric behavior of BiV ceramics obtained from powders containing nanocrystallites, prepared by mechanical milling) but also to the presence of impurity phases apart from major BiV phase that are present in the SBO glass matrix. It is known that the dielectric and polar properties and the nature of the phase transitions in ceramics are sensitive to microstructure.[21] In an attempt to bring out an analogy between the dielectric behavior of glass nanocomposites and the ceramics that exhibit diffused phase transition (DPT) behavior, we rationalized the nature of the phase transition using a procedure that is generally adopted for the ceramics, which exhibit DPT characteristics.

The phase transition occurring in ferroelectric materials could be predicted from a plot of $1/\varepsilon_r$ *vs.* T. Fig. 7(*a*) and (*b*) show the plots of $1/\varepsilon_r$ *vs.* T for both 720 and 820 K heat-treated samples, respectively. For the 720 K heat-treated sample a linear region is observed above 845 K at 1 kHz indicating that the dielectric constant obeys the Curie–Weiss law. Even in the case of the sample heat-treated at 820 K, similar behavior was observed above 770 K. In order to explain this kind of behavior (ferroelectric with diffused phase transition) the curves that are shown in Fig. 7(*a*) and (*b*) can be divided into three regions. The first region represents ferroelectric behavior up to the transition T_c, the second region near the transition indicates a diffused transition up to a temperature T_{cw} and the third region represents the linear behavior of $1/\varepsilon_r$ *vs.* T in the paraelectric phase following the Curie−Weiss relation. It is clear from the above figures that for both the samples at $T > T_{cw}$ a normal Curie–Weiss behavior is found. The difference $\Delta T_m = T_{cw} - T_c$ is indicative of the degree of thermal diffuseness. The Curie–Weiss temperature T_o is obtained by extrapolating the third region to the temperature axis and Curie–Weiss constant (C_{cw}) is calculated from the slope of curve in the third region. The various constants are listed in Table 3. The existence of a distribution of the chemical compositions in the present glass nanocomposite has prompted us to fit the dielectric constant and temperature according to eqn. (5).

$$1/\varepsilon_r = 1/\varepsilon_m + (C')^{-1}(T - T_c)^{\gamma} \quad (5)$$

Here C' is the Curie like constant, γ is the critical exponent which normally has a value between 1 (normal ferroelectric) and 2 for complete DPT,[22] and ε_m is the peak dielectric constant. In order to check whether the present system obeys a relation of this kind, a plot of log $(1/\varepsilon_r - 1/\varepsilon_m)$ *vs.* log $(T - T_c)$ were generated at 1 kHz for the 720 K and 820 K heat-treated samples [Fig. 8(*a*) and (*b*)]. The values of γ (slope), the indicator

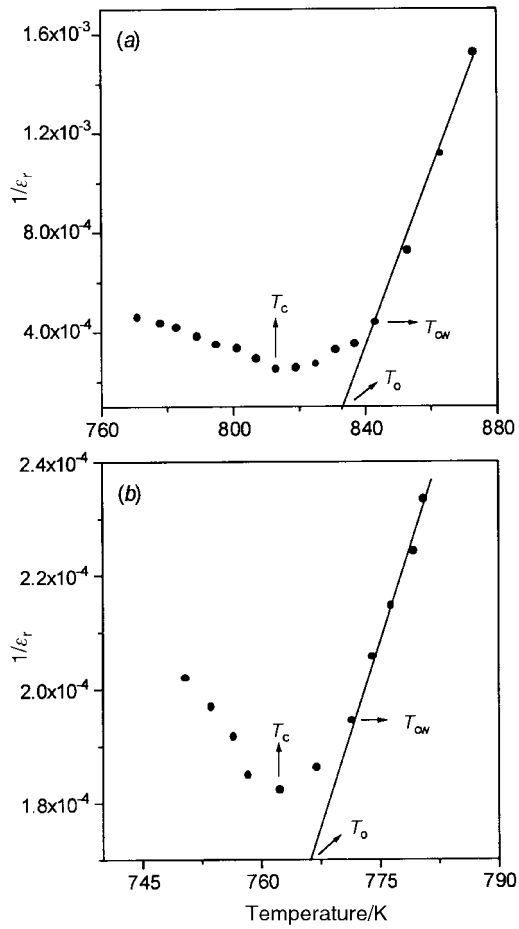

Fig. 7 Plot of $1/\varepsilon_r$ *vs.* T, for (*a*) 720 K heat-treated and (*b*) 820 K heat-treated 50 BO–50 BiV glass nanocomposites at 1 kHz.

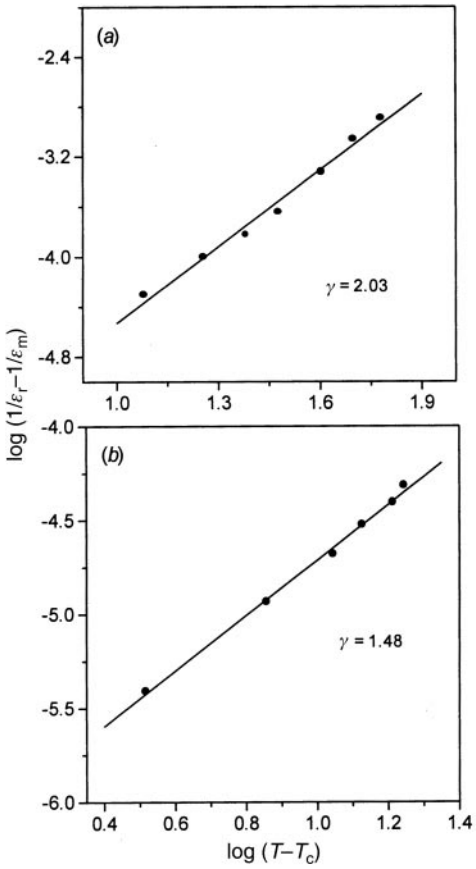

Fig. 8 Plot of $\log(1/\varepsilon_r - 1/\varepsilon_m)$ *vs.* $\log(T - T_c)$, for (*a*) 720 K heat-treated and (*b*) 820 K heat-treated 50 BO–50 BiV glass nanocomposites at 1 kHz.

of degree of diffuseness and C' (from the intercept) were computed using linear regression and included in Table 3. The value of γ in the case of the 720 K (15 nm sized crystallites) heat-treated sample is found to be 2.03 at 1 kHz and the corresponding value of C' is 3.6×10^6 whereas the values of γ and C' for the 820 K heat treated sample (40 nm sized crystallites) are 1.47 and 1.5×10^6, respectively. It is also observed that γ increases with increase in frequency for both the samples, indicating that the broadening effect is more pronounced at higher frequencies.

The mechanism of DPT in ferroelectric materials is known to be generally associated with compositional inhomogenities or other structural defects. The present glass nanocomposites have similar characteristics that are likely to impose DPT behavior. The diffuseness in the dielectric property in the vicinity of the phase transition temperature of the present samples may originate from the irregular distribution of charged defects/impurities[23,24] (in the present case impurity phases such as $BiVO_4$ and $Bi_{12}V_2O_{23}$) which may lead to the large scale potential/polarization fluctuations. Since the glass nanocomposite materials in the present study are assumed to be congregates of nano/micro regions with different compositions, the phase transition is diffused over a temperature range rather than at a single temperature and hence the observed DPT behavior.

Table 3 Parameters T_c, T_o, T_{cw}, ΔT_m, C_{cw}, γ and C' for 50 SBO–50 BiV samples heat-treated at 720 and 820 K

Curie–Weiss parameters	Heat-treated at 720 K (1 kHz)	Heat-treated at 820 K (1 kHz)
T_c/K	812	763
T_o/K	833	767
T_{cw}/K	843	771
ΔT_m/K	31	8
C_{cw}	2.50×10^4	2.63×10^5
γ	2.03	1.47
C'	3.6×10^6	1.5×10^6

Ferroelectric hysteresis loop studies

The composite 50 SBO–50 BiV heat-treated at 820 K/8 h did not show a P *vs.* E hysteresis loop at 300 K indicating the coercive field that is required to switch the polarization at room temperature is much higher. However, the same samples exhibited moderately good hysteresis loops in the range 670–760 K (in the vicinity of the ferroelectric-to-paraelectric transition temperature) [Fig. 9(*a*)] associated with a remnant polarization (P_r) of 5.63×10^{-9} C cm^{-2} and coercive field (E_c) 1250 V cm^{-1} (at 720 K) (whereas the values of P_r and E_c for a BiV ceramic containing micrometer sized crystallites are 2.25×10^{-8} C cm^{-2} and 650 V cm^{-1}, respectively).[25] These loops disappeared and the plots became linear [Fig. 9(*b*)] at 780 K, which is beyond the phase transition temperature (760 K). On cooling, the loops reappeared around 730 K, a feature that is akin to that of the ferroelectric behavior of parent BiV ceramic.

Conclusions

The nanocrystallization of ferroelectric BiV in SBO glass matrices has been demonstrated. The as-quenched and heat-treated samples were found to exhibit broad dielectric anomalies in the vicinity of the ferroelectric-to-paraelectric transition temperature of the parent polycrystalline BiV

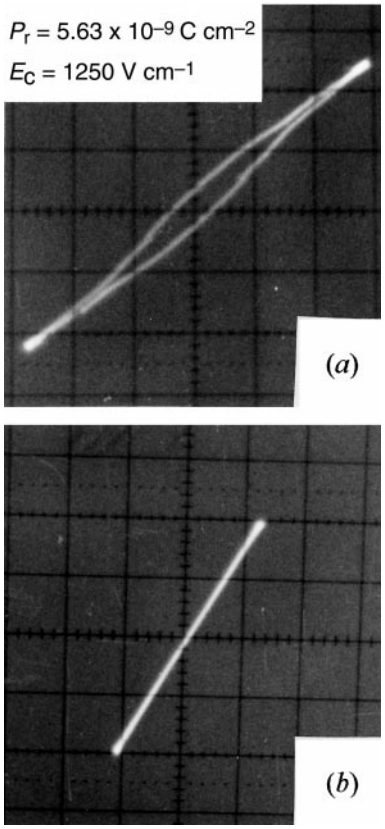

Fig. 9 *P vs. E* hysteresis loops recorded on 820 K heat-treated 50 SBO–50 BiV glass nanocomposite at two different temperatures: (*a*) 720 K and (*b*) 780 K.

phase. The dielectric anomaly is rationalized in terms of diffused phase transition formulae. The dielectric constant of the title composite is predicted using various dielectric mixture formulae and the values that are obtained using the Maxwell's equation and logarithmic mixture rule are found to be in close agreement with the experimental values. The most interesting aspect of the present investigations is the demonstration of ferroelectric behavior of these composites in the range 670–760 K.

Acknowledgements

The authors thank the Council of Scientific and Industrial Research (CSIR), Government of India for a financial grant. One of the authors (N.S.P) also acknowledges the University Grant Commission, Government of India, for the research fellowship.

References

1 J. C. Burfoot and G. W. Taylor, *Polar Dielectrics and their Applications*, Macmillan Press, London, 1979.
2 K. Shantha and K. B. R. Varma, *J. Mater. Res.*, 1999, **14**, 4651.
3 V. N. Borlsov, M. Yu. Poplavko, P. B. Avakyan and V. G. Osipyan, *Sov. Phys. Solid State.*, 1988, **30**, 904.
4 K. B. R. Varma, G. N. Subbanna, T. N. Guru Row and C. N. R. Rao, *J. Mater. Res.*, 1990, **5**, 2718.
5 K. V. R. Prasad and K. B. R. Varma, *J. Phys. D: Appl. Phys.*, 1991, **24**, 1858.
6 F. Abraham, M. F. Debreuille Gresse, G. Mairesse and G. Nowogrocki, *Solid State Ionics.*, 1998, **28–30**, 529.
7 M. V. Shankar, K. B. R. Varma and G. N. Subbanna, *Mater. Res. Bull.*, 1996, **31**, 475.
8 M. V. Shankar and K. B. R. Varma, *J. Non-Cryst. Solids.*, 1998, **226**, 145.
9 A. A. Bush and N. Yu. Venevtsev, *Russ. J. Inorg. Chem.*, 1986, **31**, 769.
10 J. K. Sinha, *J. Sci. Instrum.*, 1965, **42**, 696.
11 H. Frolich, *Theory of dielectrics*, Clarendon Press, Oxford, 1949
12 J. C. Maxwell, *A treatise on Electricity and Magnetism*, Dover Publ. Co., New York, 1954.
13 K. Lichtenecker, *Phys. Z.*, 1929, **30**, 805.
14 K. Lichtenecker and K. Rother, *Phys. Z.*, 1938, **32**, 255.
15 G. Arlt, G. Hennings and G. De. With, *J. Appl. Phys.*, 1985, **58**, 1619.
16 W. R. Bussen, L. E. Cross and A. K. Goswami, *J. Am. Ceram. Soc.*, 1966, **49**, 33.
17 H. T. Martirena and J. C. Burfoot, *J. Phys. C: Solid State Phys.*, 1974, **7**, 3182.
18 T. Kanata, T. Yoshikawa and K. Kubota, *Solid State Commun.*, 1987, **62**, 765.
19 L. E. Cross, *Ferroelectrics.*, 1994, **151**, 305.
20 B. Jimenez, J. De. Frutos and C. J. Alemany, *J. Phys. Chem. Solids.*, 1987, **48**, 877.
21 K. V. R. Prasad, A. R. Raju and K. B. R. Varma, *J. Mater. Sci.*, 1994, **29**, 2691.
22 K. Uchino and S. Nomura, *Ferroelectr. Lett.*, 1982, **44**, 55.
23 L. A. Shebanov and L. V. Korzuneva, *Mater. Res. Bull.*, 1985, **20**, 781.
24 A. E. Krumins, *Ferroelectr. Lett.*, 1983, **1**, 89.
25 K. Shantha and K. B. R. Varma, *J. Am. Ceram. Soc.*, 2000, **83**, 1122.